Soft Matter

Accepted Manuscript

This article can be cited before page numbers have been issued, to do this please use: M. Agazzi, S. Herrera, M. L. Cortez, W. A. Marmisollé, C. von Bilderling, L. I. Pietrasanta and O. Azzaroni, *Soft Matter*, 2019, DOI: 10.1039/C8SM02387E.

ROYAL SOCIETY OF CHEMISTRY

rsc.li/soft-matter-journal

Continuous assembly of supramolecular polyamine-phosphate networks on surfaces: preparation and permeability properties of nanofilms

View Article Online
DOI: 10.1039/C8SM02387E

Maximiliano L. Agazzi[1], Santiago E. Herrera[1], M. Lorena Cortez[1], Waldemar A. Marmisollé[1], Catalina von Bilderling[1,2] Lía I. Pietrasanta[2,3], Omar Azzaroni[*1].

[1.] *Instituto de Investigaciones Fisicoquímicas Teóricas y Aplicadas (INIFTA), (UNLP, CONICET), Sucursal 4, Casilla de Correo 16, 1900 La Plata, Argentina.*
[2.] *Departamento de Física, Facultad de Ciencias Exactas y Naturales, Universidad de Buenos Aires, C1428EHA Buenos Aires, Argentina.*
[3.] *Insituto de Física de Buenos Aires (IFIBA), (UBA, CONICET), C1428EHA Buenos Aires, Argentina.*

**E-mail: azzaroni@inifta.unlp.edu.ar.*

Abstract

Supramolecular self-assembly of molecular building blocks represents a powerful "nanoarchitectonic" tool to create new functional materials with molecular-level feature control. Here, we propose a simple method to create tunable phosphate/polyamine-based films on surfaces by successive assembly of poly(allylamine hydrochloride) (PAH)/phosphate anions (Pi) supramolecular networks. The growth of the films showed a great linearity and regularity with the number of steps. The coating thickness can be easily modulated with the bulk concentration of PAH and the deposition cycles. The PAH/Pi networks showed chemical stability between pH 4 and 10. The transport properties of the surfaces assemblies formed from different deposition cycles were evaluated electrochemically by using different redox probes in aqueous solution. The results revealed that either highly permeable films or efficient anion transport selectivity can be created by simply varying the concentration of PAH. These experimental evidence indicates that this new strategy of supramolecular self-assembly can be useful for the rational construction of single polyelectrolyte nanoarchitectures with multiple functionalities.

Introduction

The design of new functional materials based on surface coatings continues to be a great challenge for the scientific and technological community. Ariga and co-workers introduced the concept of "nanoarchitectonics" to describe the development of interfacial multicomponent architectures through the integration of different molecular building blocks in well-defined organized assemblies.[1-7] One of the most powerful strategies used to create multifunctional films is the layer-by-layer (LbL) assembly technique developed by Gero Decher and his collaborators in the

early 1990s.[8,9] This technique is based on the step by step adsorption of oppositely charged polyelectrolytes on surfaces and allows the control of structure, composition and film properties.[10-13] Over the last decades, the frontiers of surface science have been expanded by the appearance of bioinspired strategies like the spontaneous surface assembly of simple molecules by non-covalent interactions. In this context, Messersmith *et al.* reported and explored a process inspired by dopamine self-polymerization in mussels to build thin films of polydopamine adhered to different surfaces.[14-16] More recently, ultrathin films based on the electrostatic self-assembly of complexes formed by poly(allylamine hydrochloride) (PAH) and anions phosphate (Pi), have been generated and explored for different applications such as redox-active surfaces, electroless metallization, biorecognition, and cell adhesion.[17,18] Supramolecular interactions between polyamines with phosphate anions are present in a significant number of biological and natural processes. [19-24] In previous works, it was demonstrated that the weak polycation poly(allylamine hydrochloride) (PAH) is anionically cross-linked in the presence of single phosphate anions (Pi) forming soft particles of variable size.[25-27] Some reports reveal that these aggregates are stabilized by a combination of electrostatics and hydrogen bonding forces.[28,29]

PAH/Pi films are similar to those obtained by LbL assembly, in the sense that both platforms are constituted by a complex matrix of polyelectrolyte chains. However, in most cases, two polyelectrolytes with opposite charges are required for the traditional LbL assembly and the modulation of the film thickness is mainly attained by changing the number of deposition cycles.[30] In contrast, PAH/Pi platforms generates an ionically cross-linked network from a sole polycation and a single phosphate anion a by a one-step technique, by the simple immersion of the substrate in aqueous solution of the PAH and Pi mixture. In addition, it was observed that the PAH/Pi film thickness can be varied with the concentration of PAH in the mixture, and that its growth is limited for the self-assembly time, reaching a plateau where no more deposition of material is recorded.[17]

In this way, bioinspired assembly of PAH/Pi networks results in a platform based on a single polycation cross-linked supramolecularly. This possibility to build films constituted of a single polymer can be useful since the properties of the material are mainly those of the individual polymer, unlike the materials that integrate several macromolecular components.[31,32] One-component cross-linked platforms with modulable thickness have been previously reported, however in all cases covalent chemistry was required. Generally, single-polymer hydrogels have been built from the LbL assembly of two polyelectrolytes by a hydrogen bonding.[33] The polymer of interest was covalently cross-linked and then the other polymer was removed by some specific trigger, such as exposure to basic pH solutions.[34-39] In addition, single polyelectrolyte multilayers have also been designed by covalent LbL assembly of the same polymer using a covalent cross-linking agent between each deposition step.[40-44]

Herein, we extended the concept of the PAH/Pi assemblies by focusing on the possibility of building tunable phosphate/polyamine-based platforms from specific interactions between multiple PAH/Pi networks deposited in continuous assembly steps. The growth of the films for different deposition steps and the variation of the PAH bulk concentration was analyzed. Besides, the response of the assembly to a specific stimulus such as pH changes was also explored. Last, the transport properties of the obtained polymer coatings were electrochemically studied by monitoring the diffusion of redox probes into the film. Experimental data showed that the supramolecular integration of PAH/Pi networks by multiple assembly steps provides a simple strategy to rationally construct single polyelectrolyte nanoarchitectures with interesting controlled properties for multiple applications.

Experimental

Chemicals

Polyallylamine hydrochloride (PAH) (ca. 58 kDa), cysteamine hydrochloride, (3-aminopropyl) triethoxysilane (APTES), phosphate buffered saline (PBS), ferrocenemethanol (FcOH) and hexaammineruthenium(III) chloride were purchased from Sigma-Aldrich. Ethanol, NH_4OH, NaOH and hydrochloric acid (HCl) were purchased from Anedra. KH_2PO_4 from Carlo Erba, potassium hexacyanoferrate (III) from Biopack and hydrogen peroxide (100 vol.) from Cicarelli.

The pH of the stock solutions of Pi (10 mM KH_2PO_4) and PAH (1 mg mL^{-1}) were adjusted to 7 by adding 10% NaOH. Also, the Pi solutions were adjusted to basic pH with 10% NaOH. Acid solutions of Pi were adjusted with aqueous HCl solution (10 mM). All chemicals were of analytical grade. Water used in all experiments was purified by a Millipore system and its resistivity was 18.2 MΩ cm.

PAH/Pi-coated substrate preparation

PAH/Pi-coated substrates were fabricated from stock solutions of PAH and Pi (KH_2PO_4), both at pH = 7. The substrate was placed vertically in the interior of the modification cell and equal volumes of PAH (0.1 and 0.4 mg mL^{-1}) and Pi solutions (10 mM) were added. After 15 minutes of deposition, the substrate was washed with Pi (10 mM) for another 5 minutes. This process was repeated to obtain PAH/Pi films with different assembly steps.

Gold-sputtered glass slides modified with cysteamine were used as substrates for surface plasmon resonance and electrochemical experiments. APTES-modified Si slides were used as substrates for AFM measurements. For cysteamine modification, Au substrates were typically

soaked overnight in a 2 mM cysteamine ethanolic solution. Then, substrates were thoroughly rinsed with ethanol and water, and dried under a stream of nitrogen gas.

View Article Online
DOI: 10.1039/C8SM02387E

Si substrates were incubated in an ethanolic solution of 2% APTES for 1 h, rinsed with ethanol and annealed for 2 h at 120 °C.

Surface Plasmon Resonance

SPR detection was carried out using a SPR-Navi 210A setup (BioNavis Ltd, Tampere, Finland). SPR gold sensors were cleaned by immersion in boiling NH_4OH (28%)/H_2O_2 (100 vol) 1:1 for 15 min and then rinsed with water and ethanol. Then, they were modified with cysteamine. An electrochemistry flow cell (SPR321-EC, BioNavis Ltd.) was employed for all measurements. The injection was performed manually and SPR angular scans (two wavelength mode) were recorded with no flow in the cell. The temperature was kept at 20 °C. All SPR experiments were processed using the BioNavis Data viewer software.

Atomic Force Microscopy

Si substrates modified with APTES and coated with $(Pi/PAH)_n$, where n is the number of deposition cycles (n = 1, 4, 7 and 10), were analyzed by Atomic Force Microscopy (AFM). A Bruker Multimode AFM connected to a Nanoscope V controller was used to image the topography of the substrate. AFM tapping mode measurements were performed in a dry nitrogen ambient, using RTESP (Bruker, K = 40 N m^{-1}) cantilevers. Images were processed by flattening using NanoScope software to remove the background slope. The roughness RMS value of each image was obtained with the NanoScope software.

For the thickness measurement, AFM scanning was first performed in contact mode at high forces, removing all polymer to expose bare silicon.Sectional analysis of several profiles from a subsequent zoomed out tapping mode scan was used to evaluate the thickness.

Size and zeta potential measurements

Size of PAH/Pi complexes was determined by Dynamic Light Scattering (DLS) employing a Zetasizer Nano (Nano ZSizer-ZEN3600, Malvern, U.K.) at 25ºC employing a distribution fitting method. The zeta potential was determined from the electrophoretic mobility measured by Laser Doppler Velocimetry with a Zetasizer Nano. Measurements were performed using disposable capillary cells (DTS 1061 1070, Malvern) at 25ºC with a drive cell voltage of 30 V and employing the monomodal analysis method.

Electrochemical measurements

Cyclic voltammetry experiments were performed using a Gamry REF600 potentiostat and a conventional three-electrode cell equipped with an Ag/AgCl (3 M KCl) reference electrode and a platinum counter electrode. Cyclic voltammograms of $Fe(CN)_6^{4-}$, $Ru(NH_3)_6^{3+}$ and FcOH in Phosphate Buffered Saline (PBS: 10 mM Pi, 2.7 mM KCl, 137 mM NaCl, pH 7.4) were registered on Au/cysteamine (Au/cys) substrates modified with $(PAH/Pi)_n$ assemblies (n = 0, 1, 2, 3, 4 and 5). Cyclic voltammograms presented are those obtained in the third cycle of a total of five consecutive cycles of the potential. The peak current showed a very high stability with the number of cycles, with which the deviation standard between each magnitude was negligible.

Results and Discussion

The construction of multiple PAH/Pi networks in solid substrates were conducted through successive deposition steps (Figure 1). The formation of the films was monitored by SPR measurements. Au sensors were first chemically modified with cysteamine to confer a net positive charge to the substrate. PAH and Pi solutions at pH 7 were mixed and immediately injected to the SPR cell. After 15 minutes of deposition, the substrate was rinsed with Pi solution for another 5 minutes. This methodology was repeated for each new assembly step. The growth of the films was monitored for different concentrations of PAH (0.01, 0.025, 0.05, 0.1 and 0.2 mg mL^{-1}) in 5 mM Pi.

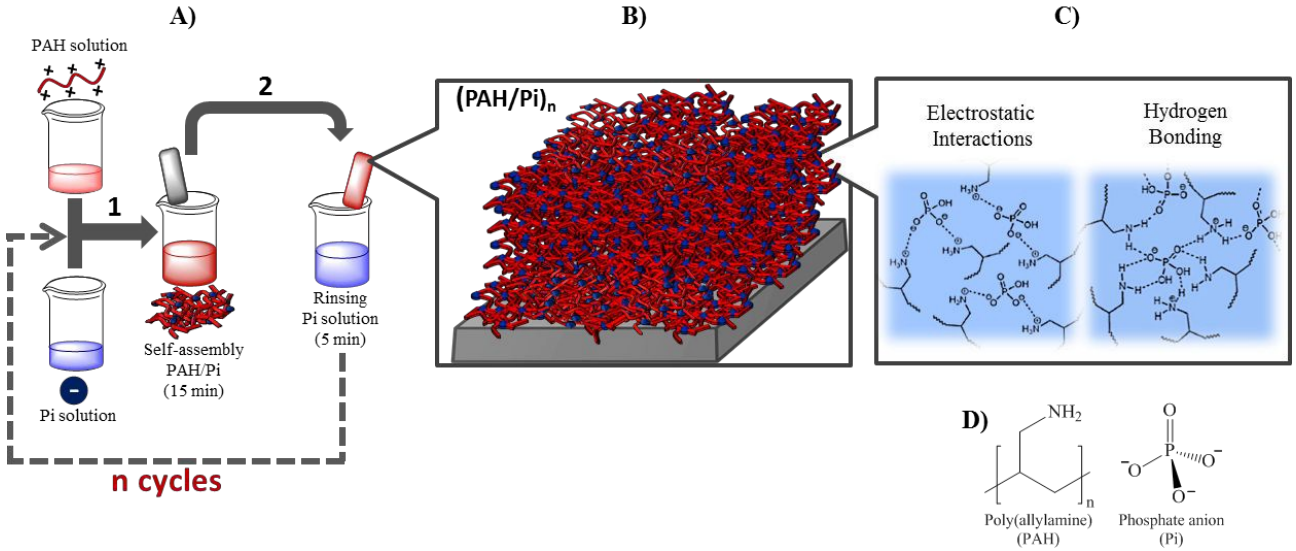

Figure 1. A) Representation of the assembly procedure for surface modification with polyamines and phosphate ions, B) simplified representation of PAH/Pi networks after n cycles of assembly, C) interaction mechanism between PAH and Pi species and D) chemical structures of PAH and Pi.

Figure 2 shows the evolution of the angle of minimum reflectivity of the Au-cys modified SPR sensors during the assembly of the PAH/Pi networks for ten injection cycles. The obtained sensograms indicate that the films based on multilayers of PAH/Pi networks grow effectively and the deposited material remains stable after each washing step. This stability indicates that this

supramolecular architecture is sustained by specific interactions between the PAH chains and phosphate anions. This continuous growth suggests that after each assembly cycle, some amine groups and phosphate anions in the deposited network remains free to interact by electrostatic interactions and hydrogen bonding with the new PAH/Pi complexes, which becomes integrated in the next cycle (Figure 1C). Hydrogen-bond interactions between amino groups and phosphate anions have been widely recognized in a variety of supramolecular systems. On one side, they have been postulated as responsible for the tridimensional stabilization of the nuclear aggregates of polyamines.[45] On the other hand, Kooijman and co-workers have also shown that the hydrogen bond interaction between amine groups of proteins and phospholipids induces further dissociation degree of phosphate moieties, increasing the protein binding interaction on the lipidic membranes. [46] The presence of hydrogen bonding between ammonium groups and phosphate anions has been also employed for explaining the specific binding of phosphates on amino-modified surfaces.[47] The relative importance of this interaction has been used to justify the much higher affinity for phosphate species as compared to other anions.

Moreover, the importance of hydrogen-bond interactions has been extensively recognized in the formation of aggregates between polyamines and phosphates,[48] as this type of interactions favors the formation of tridimensional networks.[49] In this case, the possibility of setting a hydrogen bond network seems to be essential as orthophosphate anion meets both the structural geometric requirements and ability to form hydrogen bonds. It has been shown that phosphate forms aggregates with PAH more efficiently than other divalent anions and it has been suggested the possibility of additional proton dissociation induced by interaction with protonated amines of PAH.[50]

The formation of hydrogen bonding has been also argued as responsible for the high and specific association between phosphate anions and amine groups of PAH-modified silica microparticles,[51] where the remarkable surface charge reversion cannot be only explained by electrostatic interactions.

Furthermore, FTIR studies of PAH-Pi coatings indicate that phosphate groups are not connected as in the case of crystalline solids as KH_2PO_4 and $NH_4H_2PO_4$, but they are in a more amorphous environment, consistent with those structures depicted in Figure 1C. The same features have been reported for amorphous $NH_4H_2PO_4$ where the formation of hydrogen bonds between the ammonium and $H_2PO_4^-$ has been proved.[52]

Besides the growth mechanism, Figure 2A clearly shows that the amount of material deposited increases with the PAH concentration. In addition, it is observed that the deposition rate decreases with time over each deposition cycle, until reaching a plateau. However, the time required for reaching that plateau is smaller for lower PAH concentrations. Additionally, Figure 2B shows that changes in the minimum reflectivity angle (Δθ) depend linearly on the number of deposition cycles, evidencing a notoriously regular growth for all the assembly conditions evaluated.

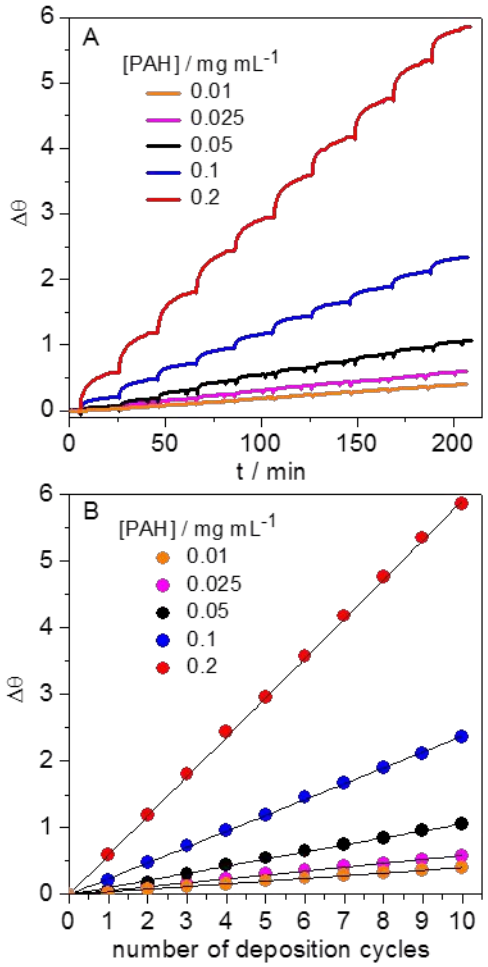

Figure 2. A) Change in the minimum reflectivity angle (Δθ) of the SPR scan (measured at λ = 785 nm) during the formation of multilayers PAH/Pi coatings on cysteamine-modified Au substrates from PAH solutions of different concentration in 5mM pH 7 Pi buffer. B) Dependence of Δθ plateau on the number of deposition cycles.

The surface coverage of the PAH/Pi complexes for each assembly cycle was estimated from SPR measurements for the different concentrations of PAH (Figure 3). The calculation was carried out using the angle change, sensitivity factors of the SPR and dn/dc = 0.16 cm^3 g^{-1} for PAH solutions.[53] These results indicate that the amount of deposed material increases exponentially with the polyelectrolyte concentration.

View Article Online
DOI: 10.1039/C8SM02387E

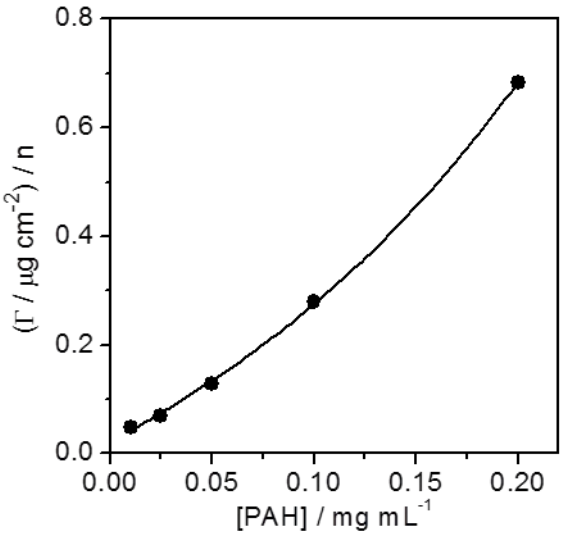

Figure 3. Dependence of surface coverage for deposition cycle on initial PAH bulk concentration.

PAH/Pi films were characterized by atomic force microscopy. For this purpose, equivalent volumes of PAH (0.4 and 0.1 mg mL^{-1}) and Pi (10 mM) solutions, both at pH 7, were mixed in a cell containing a flat silicon substrate modified with APTES. The material was deposited over the surface with the assembly methodology presented in Figure 1. AFM topographic imaging was performed on $(PAH/Pi)_n$ films formed by different deposition cycles (n: 1, 4, 7 and 10). In Figure 4 are shown AFM imaging of PAH/Pi-coatings assembled from 0.2 mg mL^{-1} PAH in 5 mM Pi pH 7. The surface topography indicated that PAH/Pi complexes are evenly distributed on the substrate generating a fairly homogeneous coating after the assembly process. In addition, images reveal the presence of important protuberances that increase in their amount and height with the deposition cycles. It was also observed that the surface roughness increases markedly with the number of deposition cycles. The RMS roughness of the PAH/Pi coatings can be estimated to be 5, 66, 85, and 95 nm for samples prepared from 1, 4, 7 and 10 cycles, respectively. Similar topographic features were observed for PAH/ Pi films formed from 0.05 mg mL^{-1} PAH in 5 mM Pi pH 7 (Figure S1).

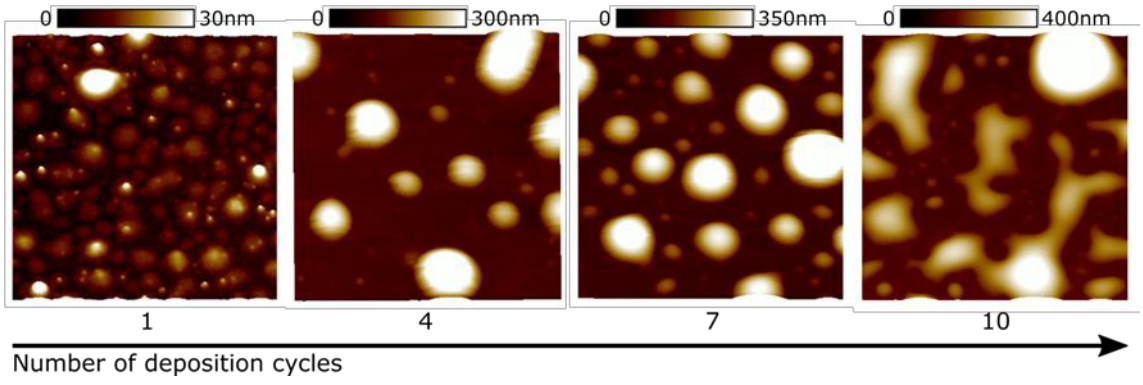

Figure 4. AFM height images of $(PAH/PI)_n$ for n=1 (RMS roughness: 5 nm), 4 (RMS roughness: 66 nm), 7 (RMS roughness: 85 nm) and 10 (RMS roughness: 95 nm). Imaging was performed in tapping mode, in dry nitrogen ambient. Z scales indicated on each image, scan size 5μm².

View Article Online
DOI: 10.1039/C8SM02387E

Additionally, the coating thickness of the film formed from 0.05 mg mL^{-1} PAH with a single deposition cycle $(PAH/Pi)_1$ was measured by AFM. For this purpose, scanning was performed in contact mode at harsh conditions (high forces), removing all polymer and exposing bare silicon (Figure S2). From this "*effective*" thickness (~2.4 nm), the refractive index of the material was estimated by adjusting the experimental SPR curves with the "Winspall" software. Using the refractive index obtained (n = 1.40), thickness values were estimated for the subsequent assembly cycles and for films with different PAH bulk concentration (Figure 5). The results show that this soft-assembly strategy of PAH/Pi networks allows to create films with nanometer-scale thickness control.

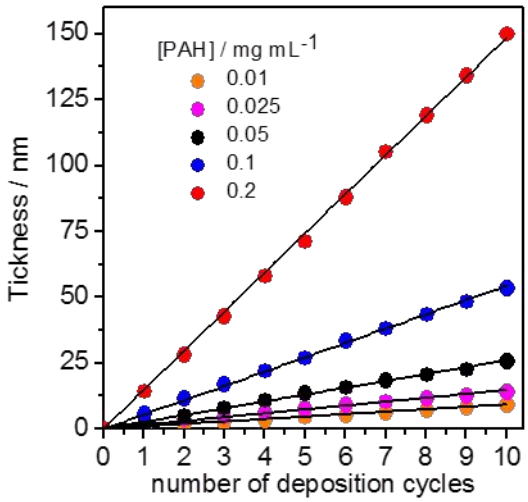

Figure 5. Thickness evolution of PAH/Pi films as a function of the number of deposited layers at different PAH bulk concentration.

So far, the results obtained allow us inferring that it is possible to construct a platform of modulable thickness based on a single ionically cross-linked macromolecular component. It is interesting to note that our approach allows us to build in mild conditions, single polymer matrices of different thicknesses based entirely on supramolecular interactions between the PAH/Pi networks generated in each assembly cycle. In a previous study, we explored a wide spectrum of functionalities for PAH/Pi films generated by a one-step self-assembly.[17] For example, simple derivatization of pendant amino groups of PAH precursors with hydroquinone and biotin provided an efficient electrochemical response and biorecognition capacity, respectively. Thus, the

possibility of modulating the film thickness would allow expanding and optimizing of the functionalities through a controlled and hierarchical organization of functional domains.

Subsequently, in order to improve our understanding of the interfacial assembly process, we studied the formation of PAH/Pi complexes in solution in the same experimental conditions as those of the SPR studies. Figure 6A shows the time evolution of the hydrodynamic diameter of PAH/Pi aggregates in solution phase, formed by adding PAH solutions (final concentrations: 0.01, 0.025, 0.05, 0.1 and 0.2 mg mL^{-1}) to a 5 mM pH 7 Pi solution. PAH/Pi colloids showed a dynamic behavior with initial sizes between 150 and 300 nm. However, when the PAH concentration was ≤ 0.1 mg mL^{-1}, a noticeable increase in size as a function of time was observed. This is due to the coagulation of the PAH/Pi colloids and the consequent formation of larger aggregates. Nevertheless, size growth is much lower in colloids formed at the highest concentration of PAH (0.2 mg mL^{-1}), showing higher stability over time. Very recently, Andreozzi *et al.* reported similar behavior in other PAH/Pi colloids.[54] It is important to emphasize that the magnitude of the hydrodynamic diameters of the PAH/Pi aggregates is much higher than the corresponding thicknesses of the films. This could indicate that the interfacial assembly is constructed mainly by the deposition of the first PAH/Pi networks complexed in solution and that the larger aggregates observed by DLS constitute the protuberances that are observed in the AFM images.

Figure 6B shows the values of the zeta potential obtained for each solution phase sample. It is known that the cross-linking of the polymer chains by the anion decreases the overall positive charge of the polyamine chains.[55] We observed that the zeta potential increases with the PAH concentration from an almost neutral potential for 0.01 mg mL^{-1} up to a positive value of around 20 mV for 0.2 mg mL^{-1}. At higher concentrations of PAH the cross-linker/polycation ratio decreases in the complexes, and the charge compensation in the polymer chains is lower. Besides, these results indicate that the growth mechanism is charge-limited. Thus, size growth can be explained by considering balance between electrostatic repulsions and van der Waals attractions.[56] A higher zeta potential makes the size smaller due to the electrostatic repulsion between the complexes, while small zeta potential decreases the repulsion, causes rapid growth and greater coagulation.

View Article Online
DOI: 10.1039/C8SM02387E

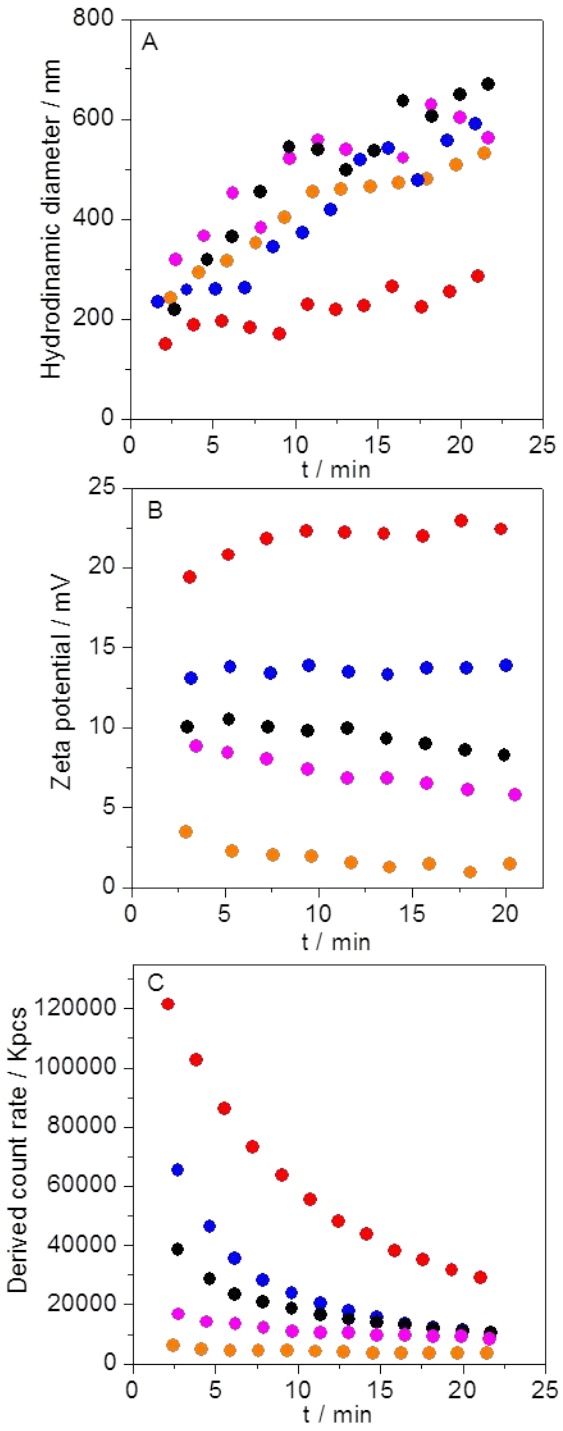

Figure 6. Time dependence of size (A), Zeta-potential (B) and derived count rate (C) of PAH/Pi colloids at the five concentrations of [PAH]: 0.2 mg mL^{-1} (red circles), 0.1 mg mL^{-1} (blue circles), 0.05 mg mL^{-1} (black circles), 0.025 mg mL^{-1} (pink circles) and 0.01 mg mL^{-1} (orange circles) in 5 mM pH 7 Pi buffer. Inset in (C): initial derived count rate for each concentration of PAH.

The time dependence of the scattered intensity is shown in Figure 6C as obtained from the derived count rate of each measurement, expressed as kilocounts (kcounts). The scattered intensity

depends on the diameter of the aggregates and the concentration of them in solution. The derived count rate decreases with time in all cases due to the coagulation and precipitation of the PAH/Pi aggregates, but for 0.2 mg mL^{-1} of PAH this decrease is lower. The inset of Figure 6C shows the variation of kcounts to the initial time as a function of PAH concentration. It is observed that the kcounts increases clearly with the concentration of polyelectrolyte, probably revealing that the concentration of PAH/Pi complex formed initially increases with the amount of PAH added. This explains that at a higher concentration of added PAH, more material is deposited on the substrate surface. In addition, the higher temporal stability of complexes formed from 0.2 mg mL^{-1} PAH may also contribute to more extended deposition processes, since the lower precipitation of aggregates allows extending the period of surface assembly. This is reflected in the sensograms of Figure 2A, where it is observed that the angle of growth does not reach a well-marked plateau after 15 minutes of deposition, as observed in other PAH concentrations.

Film Stability

The stability of the films under different pH conditions was evaluated by SPR. In many applications, it is important that functional polymeric films can be disassembled by a specific stimulus.[57] PAH is a weak polycation (effective pKa=8.5)[58] and the phosphate ion participates in three acid/base equilibria with pKa_1=2.12 ($H_3PO_4/H_2PO_4^-$), pKa_2=7.20 ($H_2PO_4^-/HPO_4^{2-}$) and pKa_3=12.36 (HPO_4^{2-}/PO_4^{3-}).[59] As the ionization degrees of PAH and Pi vary with pH, PAH/Pi films may be dissolved by pH changes. The stability with the pH of the PAH/Pi coating formed by a single deposition cycle was previously evaluated using quartz crystal microbalance, observing that PAH/Pi monolayer remain stable up to pH 3 and dissolve completely at pH 12.[17] In this sense, the pH-response of the multilayers of PAH/Pi networks was evaluated by SPR injecting Pi solutions at different pH values. We observed that the films formed from 0.05 mg mL^{-1} PAH in 5 mM Pi, were stable up to pH 4 presenting a small increase of the minimum angle, possibly due to the greater protonation of PAH that requires binding more anions for charge compensation (Figure 7A). However, at pH 3.5 the supramolecular platform starts dissolving, being completely removed at pH 2.5. At this low pH, the protonation of the Pi ions facilitates the disassembly by removal of the stabilizing electrostatic interactions between the PAH chains and the cross-linker ions. At basic pH, the polymer network remains assembled up to pH 10 and it is completely removed at pH 12 (Figure 7B). In these conditions, PAH amine groups are deprotonated causing the dissolution of the ionic network. A similar pH response was reported for macroscopic gels formed by PAH chains cross-linked by polyphosphates such as pyrophosphate anions (PPi) and tripolyphosphate (TPP).[60,61]

Coatings formed from 0.2 mg mL^{-1} PAH and 5 mM Pi show a small difference in stability in contact with acid solutions, since they are dissolved below pH 4 and completely removed at pH 3

(Figure S3). This behavior may be due to the assembly being produced from a lower PAH/Pi ratio. Thus, the supramolecular networks present a lower ionic crosslink density, generating a matrix that is more unstable to the protonation of the phosphate groups.

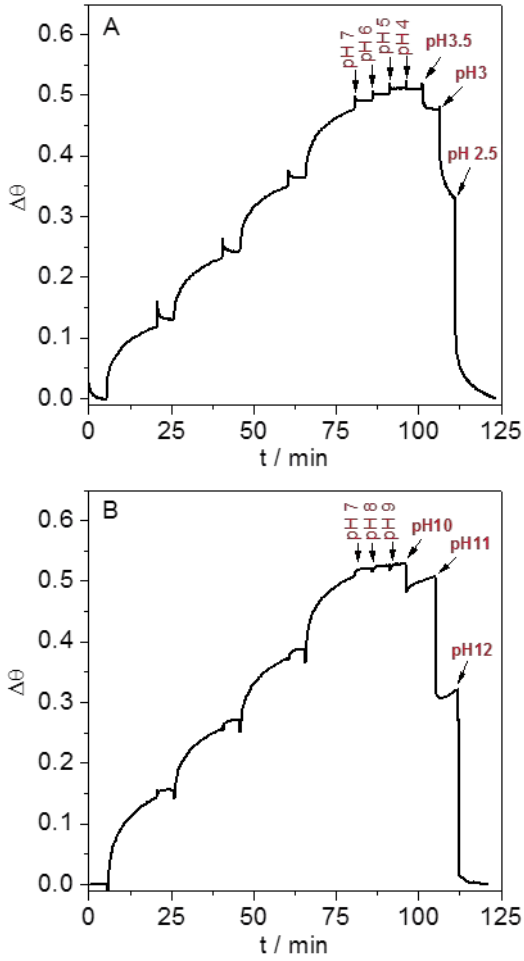

Figure 7. Change in the minimum reflectivity angle of the SPR scan (measured at λ = 785 nm) for the $(PAH/Pi)_4$ coatings (0.05 mg mL^{-1} PAH/5 mM Pi) during the injection of Pi solutions at acid pH (A) and basic pH (B).

Film Permeability

Finally, the permeability of PAH/Pi films with different assembly steps and at two bulk concentrations of PAH was analyzed. The evaluation of the transport properties of the interfacial nanoarchitectures is relevant not only to explore its structural characteristics but also because it allows guiding the study of the materials towards certain practical applications as membrane-based separations, filtration systems, sensors, bioactive release systems and biologically active coatings.[62-67] Different efforts have been made to design nanoarchitectures with suitable transport properties. Within this context, the permeability properties of LbL assemblies with the aim of

creating smart ion separation membranes have been studied.[68,69] However, for most polyelectrolyte films the ion permeability is relatively poor, due to the intrinsic charge compensation between the constituent polyelectrolytes. The ion-selectivity modulation of multilayer films was generally explored by controlling of surface charges of the assemblies.[70,71] Also, weak polyelectrolyte multilayers prepared by LbL assembly and covalently stabilized with a cross-linking agent showed ion permselectivity with pH changes.[72,73] In addition, several methods that insert a net charge and nanoporosity into films have been developed to construct ionic permselectivity membranes.[74,75]

We explored the permeability of our coatings by analyzing the electrochemical response of a film-coated electrode by cyclic voltammetry (CV) in the presence of hexacyanoferrate ($Fe(CN)_6^{3-}$) (negative probe), hexaaminoruthenium ($Ru(NH_3)_6^{3+}$) (positive probe) and ferrocene methanol (FcOH) (neutral probe) aqueous solutions. These redox probes have comparable sizes, so it is expected that the permeation is influenced mainly by the charge of each specie.[76] Electrochemical experiments were performed with 1 mM of each redox probe in PBS as supporting electrolyte. It should be noted that this medium with a high saline concentration did not affect the structural integrity of the self-assembled film (Figure S4).

Figure 8 describes the CVs of films assembled from 0.05 mg mL^{-1} PAH in 5 mM Pi pH 7, in PBS solution containing FcOH (A), $Ru(NH_3)_6^{3+}$ (B) and $Fe(CN)_6^{3-}$ (C). For comparison, the electrochemical response of the redox probes on the unmodified Au-cys electrode (black line) is also shown. It can be clearly seen, that the magnitude of the voltammetric signal, which reflects the transport of electroactive probes towards the underlying conductive support, is not affected by the presence of PAH/Pi networks with different thicknesses. The current density of the anodic peak as a function of the number of PAH/Pi deposition cycles shown in Figure 8D, reveals that the permeability of the three redox species does not change markedly with the number of assembly steps. In addition, no relevant changes are observed in the position of the redox potential, and the separation between anodic and cathodic peaks remains constant for each redox couple. This indicates that the kinetics of electron and mass transfer processes do not change with the thickness of the film regardless of the net charge of the redox probes.

View Article Online
DOI: 10.1039/C8SM02387E

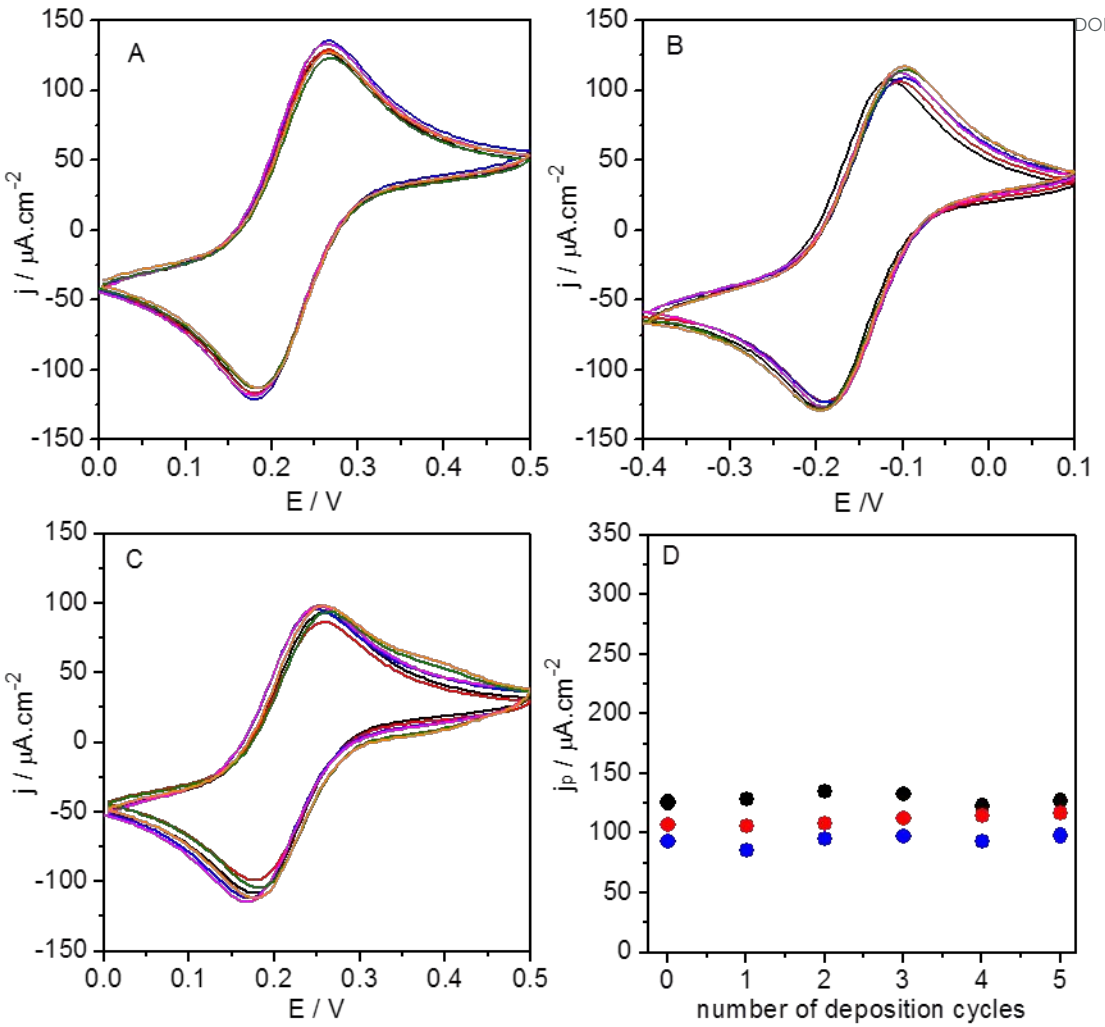

Figure 8. Cyclic voltammograms of Au/cys (black line) and Au/cys modified with PAH/Pi films formed from 0.05 mg mL^{-1} PAH in 5 mM Pi pH 7, with different numbers of deposition cycles: $(PAH/Pi)_1$ (red line), $(PAH/Pi)_2$ (blue line), $(PAH/Pi)_3$ (pink line), $(PAH/Pi)_4$ (green line) and $(PAH/Pi)_5$ (orange line), in PBS buffer containing 1 mM of (A) FcOH, (B) $Ru(NH_3)_6^{3+}$ and (C) $Fe(CN)_6^{4-}$. (D) Anodic peak current density (j_p) as a function of the number of deposition cycles for FcOH (black circles), $Ru(NH_3)_6^{3+}$ (red circles) and $Fe(CN)_6^{4-}$ (blue circles). Error bars are smaller than the symbol size. Scan rate: 0.050 Vs^{-1}

On the other hand, clear differences were observed when studying the permeation of the films formed by mixing 0.2 mg mL^{-1} PAH in 5 mM Pi pH 7 (Figure 9). In the case of $Ru(NH_3)_6^{3+}$, the permeability decreases markedly from complete permeation for $(PAH/Pi)_1$, to a practically complete suppression of the redox response for $(PAH/Pi)_5$ (Figure 9B). However, the voltammetric response in the presence of neutral FeOH shows no differences for the different coating thickness, as observed for films formed from 0.05 mg mL^{-1} PAH solutions. These results indicate that the permeation properties of the neutral probe are not affected by the amount of material deposited and, thus, the hindrance observed for the positive probe is not caused by a size exclusion mechanism.

This behavior can be understood by considering the LbL assembly concept of intrinsic and extrinsic charge compensation.[77-80] The films present an excess of protonated amines - that are not cross-linked by phosphate groups - in agreement with the positive zeta potential observed for the PAH/Pi solution phase complexes used in the surface assembly (Figure 6B). This excess of amine groups is not intrinsically compensated by electrostatic interactions with phosphate ions in the film. Considering the electroneutrality requirement, they are compensated with mobile anions from the solution. Thus, the cationic probe must diffuse through a more positive environment observing a decrease in the permeation properties by a charge exclusion mechanism. This repulsion is more intense as the amount of deposited material increases. As a consequence, the diffusion of $Ru(NH_3)_6^{3+}$ is getting slower when the deposition cycles grow. In the case of the coating formed from 0.05 mg/mL PAH, all the protonated amines groups are intrinsically compensated, generating a more neutral surface environment that does not affect the diffusion of the ionic probe.

In the case of $Fe(CN)_6^{3-}$, the electrochemical signal was stable and comparable with the unmodified electrode for all the assemblies, indicating that this anionic probe efficiently penetrates the PAH/Pi films (Figure 9C). For $(PAH/Pi)_1$ a typical reversible cyclic voltammogram is obtained with a peak separation of 80 mV. However, for $(PAH/Pi)_2$, a surface confined electron transfer process is detected by the appearing of a peak centered at 0.30-0.35 V with minimum mass transport peak separation. This signal is produced by the confinement of the redox couple produced by the interaction of $Fe(CN)_6^{3-}$ with the positively charged amine groups of the PAH chains[81]. As the number of assembly steps increases, the surface confined signal becomes more relevant. At higher thickness values, the peaks were shifted in the positive direction and the peak current density increases significantly (Figure 9D). To confirm the hypothesis, the electrode modified with PAH/Pi previously exposed to $Fe(CN)_6^{3-}$ solution was washed exhaustively. Then the CVs were recorded in a $Fe(CN)_6^{3-}$ ion-free buffer PBS (Figure S5). The peaks between 0.30-0.35 V corresponding to the electrochemical potentials of the confined species were observed, indicating that the films contain significant amounts of the redox probe. Moreover, it is also observed that the peak current decreases with the number of electrochemical cycles, suggesting that the $Fe(CN)_6^{3-}$ ions are released out of the films over time. A similar phenomenon was previously observed by Anzai *et al.* for multilayer polyelectrolyte films (PEM) generated by LbL assemblies where PAH was used as a building block.[71,82]

Taken altogether, the results allow us to infer that the PAH/Pi platforms present characteristics of hydrogel with a porous and highly hydrated polymer matrix. In addition, our architecture is completely integrated by non-covalent interactions, unlike other hydrogels reported with modulable thickness. Additionally, we note that it is possible modulate transport properties within the supramolecular network with a simple variation of the polyelectrolyte concentration in the assembly

process. Thus, the permeability of ionic species within the polymer matrix can be rationally tuned to build thin films completely permeable or with ion-transport selectivity.

View Article Online
DOI: 10.1039/C8SM02387E

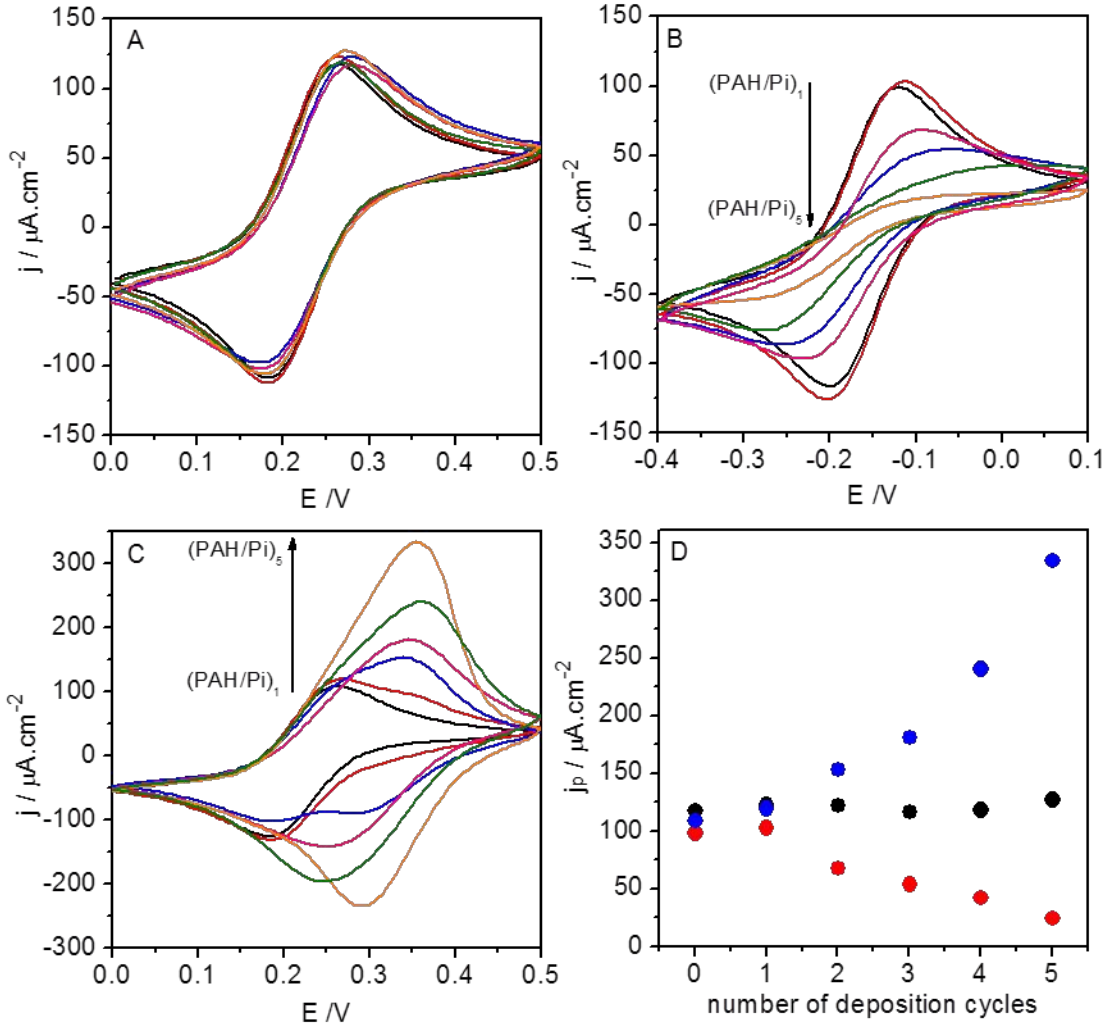

Figure 9. Cyclic voltammograms of Au/cysteamine (black line) and modified with PAH/Pi films formed from 0.2 mg mL^{-1} PAH in 5 mM Pi pH 7, with different number of deposition cycles : $(PAH/Pi)_1$ (red line), $(PAH/Pi)_2$ (blue line), $(PAH/Pi)_3$ (pink line), $(PAH/Pi)_4$ (green line) and $(PAH/Pi)_5$ (orange line), in PBS buffer containing 1 mM of (A) FcOH, (B) $Ru(NH_3)_6^{3+}$ and (C) $Fe(CN)_6^{4-}$. (D) Peak anodic current density (j_p) as a function of the number of deposition cycles for FcOH (black circles), $Ru(NH_3)_6^{3+}$ (red circles) and $Fe(CN)_6^{4-}$ (blue circles). Error bars are smaller than the symbol size. Scan rate: 0.050 Vs^{-1}

Conclusions

In this work, we further explored the bioinspired surface assembly of polyamines and phosphate anions, demonstrating that it is feasible to create entirely supramolecular nanoarchitectures with a precise structural control, through a simple and reproducible strategy based on the continuous assembly of PAH/Pi networks. We have shown that the proposed protocol enables the formation of films with highly regular growth characteristics. Thus, this new "nanoarchitectonic approach"

allows modulating the coatings thickness and the amount of material deposited, not only with the self-assembly time and the concentration of polycation but also with the assembly steps of PAH/Pi complexes.

In addition, these PAH/Pi films are pH-sensitive platforms showing entire disassembly behaviour in the presence of highly acidic or basic solutions. The transport properties of the interfacial coatings indicated that the supramolecular integrated PAH/Pi networks form a porous hydrogel matrix. Furthermore, the permeability within the polymer network can be simply modulated by varying the concentration of polyelectrolyte in the assembly solution. Thus, ultrathin films with high permeability can be constructed from low bulk concentrations of PAH. However, the increase in the concentration of PAH in the assembly mixture leads to thicker films that present an excess of extrinsically compensated protonated amines, generating a membrane with high ionic permselectivity that inhibits the transport of cationic probes.

In summary, we consider that the possibility of continuously assembling the same building blocks through controllable and flexible processes - added to the interesting and tunable properties shown by the films - opens the opportunity to rationally explore the integration and combination of different functionalities for diverse technological applications.

Acknowledgments

This work was supported by the Consejo Nacional de Investigaciones Científicas y Técnicas (CONICET, Argentina) (Grant No. PIP 0370), Agencia Nacional de Promoción Científica y Tecnológica (ANPCyT, Argentina; PICT-2013-0905 and PICT-2016-1680), the Austrian Institute of Technology GmbH (AIT–CONICET Partner Group: *"Exploratory Research for Advanced Technologies in Supramolecular Materials Science"*, Exp. 4947/11, Res. No. 3911, 28-12-2011), and Universidad Nacional de La Plata (UNLP). M.L.C., C.v.B., L.I.P., W.A.M and O. A. are staff members of CONICET. M.L.A and S.E.H. gratefully acknowledge CONICET for their postdoctoral fellowships.

References

[1] K. Ariga, M. V. Lee, T. Mori, X.-Y. Yu and J. P. Hill, *Adv. Colloid Interface Sci.*, 2010, **154**, 20-29.
[2] M. Aono, Y. Bando and K. Ariga, *Adv. Mater.*, 2012, **24**, 150-151.
[3] M. Ramanathan, L. K. Shrestha, T. Mori, Q. Ji, J. P. Hill and K. Ariga, *Phys. Chem. Chem. Phys.*, 2013, **15**, 10580-10611.

[4] (a) K. Ariga, V. Malgras, Q. Ji, M. B. Zakaria and Y. Yamauchi, *Coord. Chem. Rev.*, 2016, **320-321**, 139-152. (b) K. Ariga, M. Nishikawa, T. Mori, J. Takeya, L.K. Shrestha and J.P. Hill, DOI: 10.1080/14686996.2018.1553108

[5] (a) A. H. Khan, S. Ghosh, B. Pradhan, A. Dalui, L. K. Shrestha, S. Acharya and K. Ariga, *Bull. Chem. Soc. Jpn.*, 2017, **90**, 627-648. (b) M. Komiyama, T. Mori and K. Ariga, *Bull. Chem. Soc. Jpn.* 2018, **91**, 1075-1111.

[6] (a) K. Ariga, Y. Yamauchi, G. Rydzek, Q. Ji, Y. Yonamine, K. C.-W. Wu and J. P. Hill, *Chem. Lett.*, 2014, 43, 36-68. (b) M Komiyama, K. Yoshimoto, M. Sisido and K. Ariga, *Bull. Chem. Soc. Jpn.* 2017, **90**, 967-1004.

[7] K. Ariga, A. Vinu, Y. Yamauchi, Q. Ji and J. P. Hill, *Bull. Chem. Soc. Jpn.*, 2012, **85**, 1-32.

[8] G. Decher and J.-D. Hong and Ber. Bunsenges, *Phys. Chem*., 1991, **95**, 1430-1434.

[9] G. Decher, *Science*, 1997, **277**, 1232-1237.

[10] M. L. Cortez, N. De Matteis, M. Ceolín, W. Knoll, F. Battaglini and O. Azzaroni, *Phys. Chem. Chem. Phys.*, 2014, **16**, 20844-20855.

[11] O. Azzaroni and K. H. A. Lau, *Soft Matter*, 2011, **7**, 8709-8724.

[12] M. Ali, B. Yameen, J. Cervera, P. Ramírez, R. Neumann, W. Ensinger, W. Knoll O. Azzaroni, *J. Am. Chem. Soc*., 2010, **132**, 8338-8348.

[13] J. Irigoyen, S. E. Moya, J. J. Iturri, I. Llarena, O. Azzaroni and E. Donath, *Langmuir*, 2009, **25**, 3374-3380.

[14] H. Lee, S. M. Dellatore, W. M. Miller and P. B. Messersmith, *Science,* 2007, **318,** 426-430.

[15] H. Lee, Y. Lee, A. R. Statz, J. Rho, T. G. Park and P. B. Messersmith, *Adv. Mater.*, 2008, **20**, 1619-1623.

[16] S. M. Kang, N. S. Hwang, J. Yeom, S. Y. Park, P. B. Messersmith, I. S. Choi, R. Langer, D. G. Anderson and H. Lee, *Adv. Funct. Mater*., 2012, **22**, 2949-2955.

[17] W.A. Marmisollé, J. Irigoyen, D. Gregurec, S. Moya and O. Azzaroni. *Adv. Funct. Mater.,* 2015, **25**, 4144-4152.

[18] N. E. Muzzio, M. A. Pasquale, W. A. Marmisollé, C. von Bilderling, M. L. Cortez, L. I. Pietrasanta and O. Azzaroni, *Biomater Sci*., 2018, **6**, 2230-2247

[19] L. D´Agostino and A. Di Luccia, *Eur. J. Biochem.*, 2002, **269**, 4317-4325.

[20] N. Kroger, R. Deutzman, C. Bergsdorfm and M. Sumper. *Proc. Natl. Acad. Sci. U.S.A*, 2000, **97**, 14133-14138.

[21] A. Di Luccia, G. Picariello, G. Iacomino, A. Formisano, L. Paduano and L. D'Agostino, *FEBS J*., 2009, **276**, 2324-2335.

[22] M. Sumper, *Angew. Chem. Int. Ed*., 2004, **43**, 2251-2254.

[23] M. Sumper and N. Kroger, *J. Mater. Chem.*, 2004, **14**, 2059-2065.

[24] G. Iacomino, G. Picariello, F. Sbrana, A. Di Luccia, R. Raiteri and L. D'Agostino, *Biomacromolecules,* 2011, **12**, 1178-1186.

[25] E. Brunner, K. Lutz and M. Sumper, *Phys. Chem Chem. Phys.,* 2004, **6**, 854-857.

[26] M. Sumper, S. Lorenz and E. Brunner, *Angew. Chem. Int. Ed.*, 2003, **42**, 5192-5195.

[27] M. Mouslmani, J. M. Rosenholm, N. Prabhakar, M. Peurla, E. Baydoun and D. Patra, *RSC Adv*., 2015, **5**, 18740-18750.

[28] L. D´Agostino, M. di Pietro and A. Di Luccia, *FEBS J.*, 2005, **272**, 3777-3787.

[29] K. Lutz, C. Groger, M. Sumper and E. Brunner, *Phys. Chem. Chem. Phys.*, 2005, **7**, 2812-2815.

[30] E. Hubsch, V. Ball, B. Senger, G. Decher, J. C. Voegel and P. Schaaf, *Langmuir,* 2004, **20**, 1980-1985.

[31] V. Kozlovskaya, E. Kharlampieva, M. L. Mansfield and S. A. Sukhishvili, *Chem. Mater.*, 2006, **18**, 328-336.
[32] J. J. Richardson, B. L. Tardy, H. Ejima, J. Guo, J. Cui, K. Liang, G. H. Choi, P. J. Yoo, B. G. De Geest and F. Caruso, *ACS Appl. Mater. Interfaces*, 2016, **8**, 7449-7455.
[32] S. R. Bhatia, S. F. Khattak, S. C. Roberts. *Curr. Opin. Colloid Interface Sci*., 2005, 10, 45-51.
[33] E. Kharlampieva, V. Kozlovskaya and S. A. Sukhishvili, *Adv. Mater*., 2009, **21**, 3053-3065.
[34] E. Kharlampieva, I. Erel-Unal and A. S. Sukhishvili, *Langmuir*, 2007, **23**, 175-181.
[35] Y. Fu, S. Bai, S. Cui, D. Qiu, Z. Wang and X. Zhang, *Macromolecules*, 2002, **35**, 9451-9458.
[36] V. A. Kozlovskaya, E. P. Kharlampiev, I. Erel-Unal and S. A. Sukhishvili, *Polymer Science Ser. A*, 2009, **51**, 719-729.
[37] E.S. Dragan and F. Bucatariu, *Macromol. Rapid Commun.*, 2010, **31**, 317-322.
[38] V. A. Kozlovskayaa, E. P. Kharlampievaa, I. Erel-Unal and S. A. Sukhishvili, *Polymer Science Ser. A*, 2009, **51**, 719-729.
[39] Y. Zhang, Y. Guan and S. Zhou, *Biomacromolecules*, 2005, **6**, 2365-2369.
[40] Z. Wang, H. Zhu, D. Li and X. Yang, *Colloids Surf. A,* 2008, **329**, 58-66.
[41] F. Bucatariu, G. Fundueanu, G. Hitruc and E. S. Dragan, *Colloids Surf. A*, 2011, **380**, 111-118.
[42] U. Manna, J. Dhar, R. Nayak and S. Patil, *Chem. Commun*., 2010, **46**, 2250-2252.
[43] G. K. Such, J. F. Quinn, A. Quinn, E. Tjipto and F. Caruso*, J. Am. Chem. Soc.*, 2006, **128**, 9318-9319.
[44] W. Tong, C. Gao and H. Möhwald, *Macromol. Rapid Commun*., 2006, **27**, 2078-2083.
[45] L. D'Agostino, M. di Pietro and A. Di Luccia, *FEBS J.*, 2005, **272**, 3777–87.
[46] (a) E. E. Kooijman, D. P. Tieleman, C. Testerink, T. Munnik, D. T. S. Rijkers, K. N. J. Burger and B. De Kruijff, *J. Biol. Chem.*, 2007, **282**, 11356–11364. (b) E. E. Kooijman and K. N. J. Burger, *Biochim. Biophys. Acta - Mol. Cell Biol. Lipids*, 2009, **1791**, 881–888.
[47] (a) D. A. Capdevila, W. A. Marmisollé, F. J. Williams and D. H. Murgida, *Phys. Chem. Chem. Phys.*, 2013, **15**, 5386–94. (b) W. A. Marmisolle, D. A. Capdevila, E. De Llave, F. J. Williams and D. H. Murgida, *Langmuir*, 2013, **29**, 5351–5359.
[48] W. A. Marmisollé, J. Irigoyen, D. Gregurec, S. Moya and O. Azzaroni, *Adv. Funct. Mater.*, 2015, **25**, 4144–4152.
[49] K. Lutz, C. Gröger, M. Sumper and E. Brunner, *PCCP*, 2005, **7**, 2812–5.
[50] W. J. Dressick, K. J. Wahl, N. D. Bassim, R. M. Stroud and D. Y. Petrovykh, *Langmuir*, 2012, **28**, 15831–15843.
[51] G. Laucirica, W. A. Marmisollé and O. Azzaroni, *Phys. Chem. Chem. Phys.*, 2017, **19**, 8612–8620.
[52] (a)C. Sun and D. Xue, *J. Mol. Struct.*, 2014, **1059**, 338–342. (b)C. Sun and D. Xue, *J. Phys. Chem. C*, 2014, **118**, 16043–16050.
[53] M. Eriksson, S. M. Notley and L. Wågberg, *J. Colloid Interface Sci*., 2005, **292**, 38-45.
[54] P. Andreozzi, E. Diamanti, K. R. Py-Daniel, P. R. Cáceres-Vélez, C. Martinelli, N. Politakos, A. Escobar, M. Muzi-Falconi, R. Azevedo and S. E. Moya, *ACS Appl. Mater. Interfaces,* 2017, ***9***, 38242-38254.
[55] V. S. Murthy, R. K. Rana and M. S. Wong, *J. Phys. Chem. B*, 2006, **110**, 25619-25627.
[56] Y. Xia, T. D. Nguyen, M. Yang, B. Lee, A. Santos, P. Podsiadlo, Z. Tang, S. C. Glotzer and N. Kotov, *Nat. Nanotechnol.,* 2011, **6**, 580-587.
[57] S. Pavlukhina and S. Sukhishvili, *Adv. Drug Delivery Rev.*, 2012, **63**, 822-836.
[58] S. R. Bhatia, S. F. Khattak and S. C. Roberts, *Curr. Opin. Colloid Interface Sci*., 2005, **10**, 45-51.

View Article Online
DOI: 10.1039/C8SM02387E

[59] X. Z. Shu and K. J. Zhu. *Eur. J. Pharm. Biopharm.,* 2002, **54**, 235-243.
[60] Y. Huang, P. G. Lawrence and Y. Lapitsky, *Langmuir,* 2014, **26**, 7771-7777.
[61] P. G. Lawrence and Y. Lapitsky, *Langmuir*, 2015, **31**, 1564-1574.
[62] J. J. Keating, J. Imbrogno and G. Belfort, *ACS Appl. Mater. Interfaces*, 2016, **8**, 28383-28399.
[63] X. Liu, and M. L. Bruening, *Chem. Mater*., 2004, **16**, 351-357.
[64] M. L. Cortez, W. Marmisollé, Diego Pallarola, L I. Pietrasanta, D. H. Murgida, M. Ceolín, O. Azzaroni and F. Battaglini, *Chem. Eur. J.,* 2014, **20**, 13366 -13374.
[65] R. M. Flessner, Y. Yu and D. M. Lynn, *Chem. Commun.*, 2011, **47**, 550-552.
[66] E. Vazquez, D. M. Dewitt, P. T. Hammond and D. M. Lynn*, J. Am. Chem. Soc*., 2002, **124**, 13992-13993.
[67] L. Han, X. Lu, K. Liu, K. Wang, L. Fang, L.-T. Weng, H. Zhang, Y. Tang, F. Ren, C. Zhao, G. Sun, R. Liang and Z. Li*, ACS Nano*, 2017, **11**, 2561-2574.
[68] L. Krasemann, A. Toutianoush and B. Tieke, *J. Membr. Sci.*, 2001, **181**, 221-228.
[69] A. M. Balachandra, J. H. Dai and M. L. Bruening, *Macromolecules*, 2002, **35**, 3171-3178.
[70] R. Takita, Y. Okamura, Y. Endo and J. I. Anzai*, Electroanalysis*, 18, 2006, 1627-1630.
[71] T. Noguchi and J. I. Anzai. *Langmuir*, 2006, **22**, 2870-2875.
[72] S. E. Burke and C. J. Barrett, *Macromolecules*, 2004, **37**, 5375-5384.
[73] M. K. Park, S. Deng and R. C. Advincula, *J. Am. Chem. Soc.,* 2004, **126**, 13723-13731.
[74] J. Dai, A. M. Balachandra, J. I. Lee and M. L. Bruening, *Macromolecules,* 2002, **35**, 3164-3178.
[75] Q. Li, Q., J. F. Quinn and F. Caruso, *Adv. Mater.,* 2005, **17**, 2058-2062.
[76] J. L. Zhang, M. E. Williams, M. H. Keefe, G. A. Morris, S. T. Nguyen and J. T. Hupp, *Electrochem. Solid State Lett.,* 2002, **5**, 25-28.
[77] J.B. Schlenoff, H. Ly and M. Li, *J. Am. Chem. Soc*., 1998, **120**, 7626-7634.
[78] L. Krasemann and Bernd Tieke, *Langmuir*, 2000, **16** , 287-290.
[79] T. R. Farhat, J. B. Schlenoff. *Langmuir*, 2001, **17**, 1184-1192.
[80] Farhat, T. R. and Schlenoff, J. B. *J. Am. Chem. Soc. 2003, **125**,* 4627-4636.
[81] M. Villalba, L. P. Méndez De Leo and E. J. Calvo, *ChemElectroChem*., 2014, **1**, 195-199.
[82] R. Takita, K. Yoshida and J. I. Anzai, *Sens. Actuators B*, 2007, **121**, 54-60.

View Article Online
DOI: 10.1039/C8SM02387E

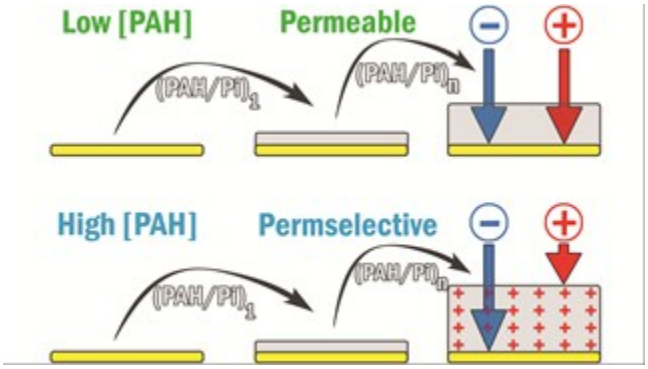

84x47mm (96 x 96 DPI)